The Role of Perisynaptic Glial Sheaths in Glutamate Spillover and Extracellular Ca^{2+} Depletion

Dmitri A. Rusakov
Institute of Neurology, University College London, London WC1N 3BG, Neurophysiology, National Institute for Medical Research, Mill Hill, London NW7 1AA, United Kingdom

ABSTRACT Recent findings suggest that rapid activation of extrasynaptic receptors and transient depletion of extracellular Ca^{2+} may represent an important component of glutamatergic synaptic transmission. These phenomena imply a previously unrecognized role for synaptic glial sheaths: to retard extracellular diffusion in the synaptic vicinity. The present study is an attempt to assess the extent and physiological implications of this retardation using a detailed compartmental model of the typical synaptic environment. The model allows reconstruction of a partial (asymmetric) glial sheath covered with transporter molecules, which gives a more realistic representation of the vicinity of central synapses. Simulations show to what extent, in conditions compatible with physiology, the occupancy of synaptic receptors and the depletion of Ca^{2+} in the cleft increase with increased glial coverage. The impact of glial sheaths on synaptic transmission is shown to become greater with smaller synapses and with slower kinetics of perisynaptic ion transients. At a calyceal synapse, a profound temporal filtering of fast Ca^{2+} influx is found, and similar phenomena are predicted to occur following simultaneous activation of multiple synapses in the neuropil. The results provide a quantitative guidance for interpretation of physiological experiments that address fast transients of neurotransmitters and small ions in the brain tissue.

INTRODUCTION

It has recently emerged that fast intersynaptic communication within cerebellar glomeruli occurs via spillover of synaptically released neurotransmitters, in particular glutamate and GABA (Mitchell and Silver, 2000a,b; Rossi and Hamann, 1998). By far the simplest explanation for such phenomena is that the glomerular envelope retains a high extracellular level of the neurotransmitters by restricting extracellular diffusion. Although this type of spatially closed synaptic formation is relatively unique, glial sheaths commonly occur near excitatory glutamatergic synapses (Spacek, 1985; Barbour et al., 1994; Shepherd and Harris, 1998; Ventura and Harris, 1999; Sykova et al., 1999). However, the relationship between glial coverage and the extent of extrasynaptic actions of glutamate and GABA remains poorly understood. This issue is not trivial: on the one hand, a closed glial envelope could retain high levels of released neurotransmitter in the synaptic vicinity; on the other hand, glial surfaces are enriched in transporter molecules (Lehre et al., 1995; Lehre and Danbolt, 1998; Schousboe, 2000) that rapidly remove glutamate (or GABA, although it is less well studied) from the extracellular space (Diamond and Jahr, 1997; Otis and Kavanaugh, 2000). Indeed, pharmacological blockade of glutamate transporters facilitates extrasynaptic communication mediated by glutamate in the hippocampus (Asztely et al., 1997), in the olfactory bulb (Isaacson, 1999), and between parallel fiber (PF) synapses in the cerebellum (Carter and Regehr, 2000).

It is not only neurotransmitter transients that can be affected by perisynaptic glia. The role of glial sheaths in spatial buffering and maintaining the homeostasis of K^+ ions has long been recognized and studied in detail (Kuffler et al., 1966; Reichenbach, 1991; Janigro et al., 1997; Araque et al., 1999). Much less is known about the effects of the glial coverage on perisynaptic fluxes of Ca^{2+} exerted by synaptic activation. Such effects may have important physiological consequences, especially because any changes in the extracellular Ca^{2+} level ($[Ca^{2+}]_o$) could alter the probability of synaptic release. Relatively slow waves of $[Ca^{2+}]_o$ in brain areas have long been shown to follow strong electrical stimulation or application of synaptic receptor agonists (Mody and Heinemann, 1986; Nicholson, 1980; Pumain and Heinemann, 1985; Nicholson and Rice, 1987). Recently, in the calyx-type synapse in the auditory brain stem, fast Ca^{2+} influx was shown to decrease following a prolonged (~100 ms) depolarization of the pre or postsynaptic membrane, which was attributed to Ca^{2+} depletion in the cleft (Borst and Sakmann, 1999). In the chick ciliary ganglion, depletion of Ca^{2+} in the synaptic cleft has explained a rise in the fast Ca^{2+} tail current (following a 100-ms depolarization) when the postsynaptic membrane was removed from the calyx (Stanley, 2000). If such depletion is common in the synaptic neuropil, this could change our understanding of the fundamental mechanisms of neural communication in the brain (Brown et al., 1995; Montague, 1996).

Because it has not been possible to measure fast perisynaptic diffusion directly, it would be useful to obtain a quantitative biophysical assessment for the effect of glial sheaths on synaptically evoked transients of neurotransmitter and Ca^{2+} ions. The relationship between the uptake and

Received for publication 8 May 2001 and in final form 11 July 2001.

Address reprint requests to Dr. Dmitri A. Rusakov, Institute of Neurology, University College London, Queen Square, London WC1N 3BG, UK. Tel.: +44-207-837-3611 ext. 4336; Fax: +44-207-278-5616; E-mail: d.rusakov@ion.ucl.ac.uk.

0006-3495/01/10/1947/13 $2.00

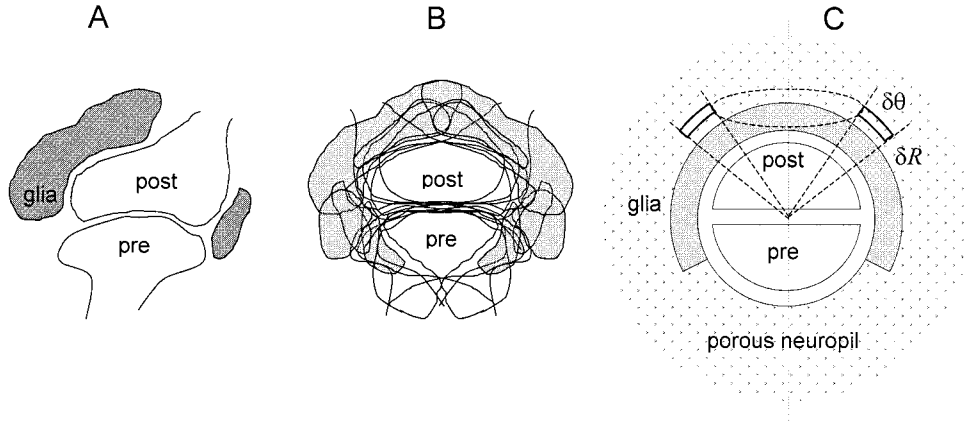

FIGURE 1 Compartmental model of the synaptic environment. (*A* and *B*) An illustration to the quantitative assessment of the typical geometry of synaptic environment, as described in detail previously (Rusakov and Kullmann; 1998a: electron micrographs of synapses are transformed into the one-pixel outline of the extracellular space profile (*A*, glial profiles shown in gray); the resulting images (a statistical sample) are aligned with respect to the cleft center, superimposed and averaged (*B*); such diagrams are used to compute the expected occurrence of the extracellular space (or glia) in the synaptic vicinity, as seen in a 2D section perpendicular to the cleft. (*C*) The resulting geometrical approximation (central planar section): the cleft separates two hemispheres surrounded by a (partial) glial sheath (shown in gray) and embedded in a porous medium. Space is partitioned in the radial (step dR) and tangential (step $\delta\theta$) directions, as indicated, with the rotational symmetry; two sections of one compartment are shown. Diffusion flux, binding, uptake, influx, and efflux are computed explicitly at each compartment and its interfaces.

the spatial profile of neurotransmitter released from a continuous local source in the neuropil has been established theoretically (Nicholson, 1995). As for nonstationary synaptic events, diffusion of rapidly released glutamate in the synaptic cleft has been investigated using analytical approaches (Uteshev and Pennefather, 1996; Kleinle et al., 1996) or Monte Carlo simulations (Bartol et al., 1991; Clements, 1996; Wahl et al., 1996; Kruk et al., 1997; Trommershauser et al., 1999). At the cerebellar parallel fiber synapse (which is often covered by glia), experimental recordings of synaptic currents indicated a retarded glutamate transient, in line with predictions of a compartmental model of the perisynaptic space (Barbour et al., 1994).

Similar simulation methodologies have been applied to assess the extent of extracellular Ca^{2+} depletion following synaptic activation (Vassilev et al., 1997; Egelman and Montague, 1998, 1999), and the role of glial ensheathment in these phenomena has been addressed analytically (Smith, 1992). However, a detailed implementation of the perisynaptic architecture and the assumption-free diffusion simulation techniques promise a more accurate assessment for the role of glial sheaths (King et al., 2000). Recently, a compartmental model was proposed that implemented the average geometric features of the perisynaptic environment in the hippocampus (Rusakov and Kullmann, 1998a; Rusakov et al., 1999). In this earlier study, however, the surrounding neuropil was considered isotropic, thus excluding from consideration the uneven occurrence of diffusion obstacles or glia near the synapse.

Here, a compartmental model is developed that accommodates uneven glial sheaths. With this model, the role of glial coverage in shaping the occupancy of perisynaptic receptors and in determining the extracellular Ca^{2+} transients is explored for the synaptic environment of small central synapses. A similar modeling approach is applied to estimate Ca^{2+} depletion at a calyx-type synapse, in relation to recent experimental findings (Borst and Sakmann, 1999; Stanley, 2000). A profound temporal filtering of fast Ca^{2+} influx is illustrated for this type of synapses, and similar phenomena are predicted to occur following activation of multiple synapses in the neuropil.

MATERIALS AND METHODS

Modeling the synaptic environment

Synaptic geometry

In an earlier study, the perisynaptic environment in hippocampal area CA1 was investigated by analyzing electron micrographs of axo-spine synapses using methods of mathematical morphology (Rusakov and Kullmann, 1998a). As described in detail in that study and also explained here in Fig. 1, the typical geometry of the synaptic environment can be represented by a synaptic cleft (radius 0.11 μm in area CA1), two hemispheric obstacles to diffusion, and a porous medium (porosity $\alpha = 0.12$, and tortuosity $\lambda = 1.4$) representing the surrounding neuropil. With this geometry, the space can be divided into small compartments allowing the multicomponent diffusion-reaction transport to be computed for kinetics of arbitrary complexity. The earlier model, however, used concentric space compartments and, therefore, was restricted to a spherically symmetric environment. The present model introduces another (tangential) dimension of space partitioning, as illustrated in Fig. 1 *C* and detailed below. Given rotational symmetry around the central synaptic axis (perpendicular to the cleft), this model allows a perisynaptic environment of arbitrary complexity.

The size of the synaptic apposition zone (the diameter of hemispheric obstacles) was initially set at 0.4 μm, to reflect the morphology of the parallel fiber synapse in cerebellum, a common excitatory synapse often surrounded by glia (Lehre and Danbolt, 1998; also Lehre and Rusakov,

unpublished observations). As explained in the Results, this size was varied to assess its impact on the perisynaptic diffusion transients.

Space compartments

The coordinate origin was set at the synaptic cleft center, the space compartments ran in the radial direction with step δR (radius $R = i\delta R$, $i = 1, \ldots, N_i$), and in the tangential (geodesic) direction with an angular step $\delta\theta$, as depicted in Fig. 1 *C*. Inside the synaptic apposition space (cleft between two hemispheres, Fig. 1 *C*), the space compartments were concentric cylindrical rings.

Outside the cleft, each ring-shaped (i, j)th compartment faced two adjacent compartments in the tangential direction (interface area $S_T(i,j) = 2\pi R(i)\sin\theta(j)\delta R$, where $\theta(j)$ is the angle between the z axis and the interface conic surface), and two in the radial direction (interface area $S_R(i, j) = 2\pi R^2(i)\{\cos\theta(j) - \cos\theta(j-1)\}$). The compartment volume was $V(i,j) = 0.5\{S_R(i,j) + S_R(I-1,j)\}\delta R$. In our simulations we used $\delta R = 20$–50 nm, $\delta\theta = \pi/9$, and $N_i = 100$–400.

Diffusion

The concentration of extracellular glutamate or Ca^{2+} within each (i, j)th compartment at time t, $C(i, j, t)$, was computed using the mass transfer balance:

$$C(i,j,t) = C(i,j,t-dt) + \{\mathbf{j}_R^{\Sigma}(i,j,t)S_R + \mathbf{j}_T^{\Sigma}(i,j,t)S_T\}\frac{dt}{V(i,j)} + (v_+ - v_-)dt \quad (1)$$

where dt is the time step; $\mathbf{j}_R^{\Sigma}$ and $\mathbf{j}_T^{\Sigma}$ are the cumulative fluxes through radial and tangential interfaces, respectively; and v_- and v_+ are the rates of the cumulative binding/influx and release/efflux, respectively, of glutamate or Ca^{2+} computed from the reactions as detailed below. At each time point t, the diffusion flux $\mathbf{j}_{AB}$ between adjacent compartments A and B was computed using Fick's 1st law:

$$\mathbf{j}_{AB}(t) = -D\nabla C = -\frac{D}{\delta s}\{C_A(t-dt) - C_B(t-dt)\}, \quad (2)$$

where δs is the spatial distance between the respective compartment centroids and D is the effective diffusion coefficient. This computational approach did not require particular solutions for the fundamental diffusion equation (Fick's 2nd law) to be explicitly derived, and could in principle adopt arbitrary reaction kinetics of the diffusing substances. At each time step the total amount of the diffusing substance in the system was computed, as described below, to test compliance with the mass conservation law. In the modeled environment, the cutoff distance (at which glutamate and Ca^{2+} levels were clamped at their resting values) was 5 μm for small synapses and 20 μm for the calyx-type synapse.

The two synaptic hemispheres were separated from the surrounding porous neuropil by a 25-nm extracellular gap (free medium). To account for the free-to-porous medium transition, the outward flux (diffusion source strength) was increased by scaling $\mathbf{j}$ up to $\mathbf{j}/\alpha$ while the apparent diffusion coefficient D was scaled down as D/λ^2. Given these adjustments, Eqs. 1 and 2 are equivalent to diffusion equations applied by Nicholson for the porous neuropil (Eqs. 3–5 in Nicholson, 1995).

Glial sheath and glutamate transporter density

Three characteristic cases of glial coverage were considered: 1) no glial coverage; 2) one-half of the synapse (hemispheric obstacles) is covered; and 3) ~95% of the synapse is covered, leaving a single escape route for glutamate (at the synaptic "pole"), as illustrated in Fig. 2, *A1–3* and Fig. 3, upper panel diagrams. The thickness of the glial sheath was set at 100 nm to reflect the minimum width of glial profiles observed in electron micrographs (representing thin planar sections of 3D cell protrusions). The sheath was modeled explicitly by setting the impermeable walls at the corresponding space compartments embedded in the porous neuropil.

The surface density of major glutamate transporters (GLAST/GLT) in glial membranes was set in the range of $\sim 5 \cdot 10^3$ μm^{-2} (hippocampal astrocytes) to $\sim 10^4$ μm^{-2} (Bergmann glia in cerebellum), in agreement with data of quantitative immunoblotting combined with specific immunoelectron labeling (Lehre and Danbolt, 1998). Given an average extracellular gap of ~20 nm, this corresponds to a concentration of 0.5–1.0 mM within the extracellular space adjacent to the glial surface. Because the physiologically available transporters probably represent only a proportion of the cytochemically identified molecules, the level of 0.5 mM was accepted in the present model. The transporters were distributed uniformly, as suggested by experimental data (Lehre and Danbolt, 1998) at this level in the space compartments adjacent to the glial sheath surface.

Kinetics of glutamate release and uptake

Five thousand molecules of glutamate (Bruns and Jahn, 1995) were released into the central compartment $(i, j = 1)$ with an α-function rate $\sigma^2 t\exp(-\sigma t)$, where $\sigma = 39$ ms^{-1} (Stiles et al., 1996). Accounting for the possible effects of macromolecular obstacles (Rusakov and Kullmann, 1998b), the diffusion coefficient of glutamate in the cleft was initially set at $D = 0.3$ μm^2/ms (which was further reduced by the neuropil tortuosity outside the cleft), and further tests were carried out for the likely physiological limits of D, 0.1 μm^2/ms and 0.6 μm^2/ms, as described below.

Although glutamate uptake has complex, multi-stage kinetics (Diamond and Jahr, 1997; Otis and Kavanaugh, 2000; Auger and Attwell, 2000; Otis and Jahr, 1998), its ultimate effect on the extracellular level can be represented by the reaction:

$$Glu + T \underset{k_{-1}}{\overset{k_1}{\longleftrightarrow}} GluT \xrightarrow{k_2} Glu_{in} + T \quad (3a)$$

where k_2 also represents the reappearance of free binding sites on the cell surface over the full uptake cycle. The kinetic constants were set in accordance with the characteristic parameters of GLT/GLAST glutamate transporters estimated in studies of cloned glutamate transporters using oocytes (Arriza et al., 1994; Wadiche et al., 1995) or evoked uptake currents in glial cells (Diamond and Jahr, 1997; Bergles and Jahr, 1998) or in inside-out membrane patches (Mennerick et al., 1999; Otis and Jahr, 1998; Bergles and Jahr, 1998): $k_1 = 10^4$ M^{-1} ms^{-1} and $k_{-1} = 0.2$ ms^{-1}. The cycling rate was set at its upper limit at 36°C, $k_2 = 0.1$ ms^{-1} (Bergles and Jahr, 1998), to reflect a conservative estimate for extracellular glutamate transients.

The reactions in Eq. 3a involve a set of kinetic equations, which were implemented as a straightforward finite-difference scheme for every (i,j)th compartment:

$$[Glu]_t = [Glu]_{t-dt} + (k_1[Glu]_{t-dt}[T]_{t-dt} + k_{-1}[GluT]_{t-dt})dt \quad (3b)$$

$$[GluT]_t = [GluT]_{t-dt} + \{(-k_1 + k_2)[GluT]_{t-dt} + k_1[Glu]_{t-dt}[T]_{t-dt}\}dt \quad (3c)$$

$$[GluT]_t + [T]_t = [GluT]_{t-dt} + [T]_{t-dt} = [T_{tot}] \quad (3d)$$

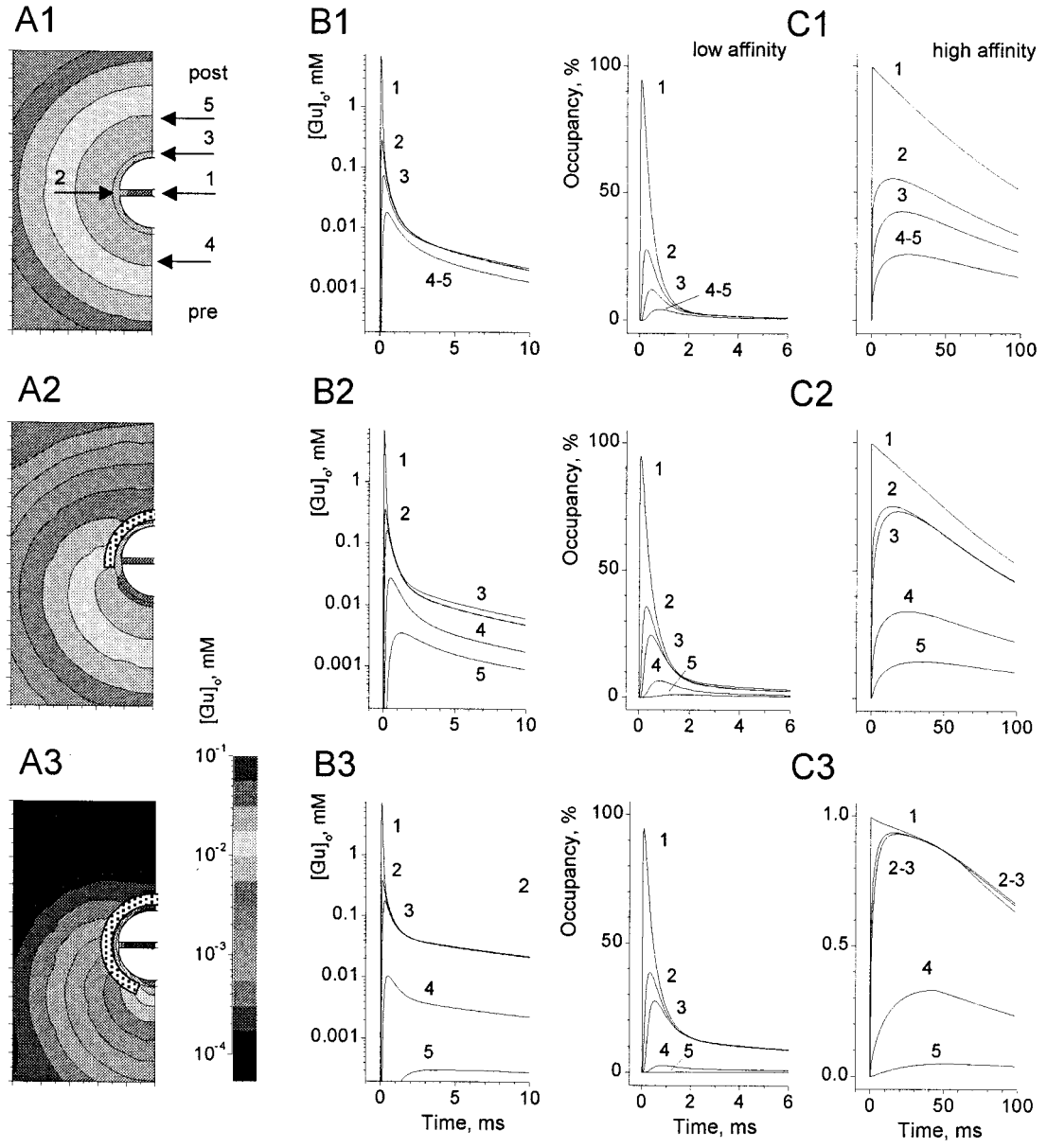

FIGURE 2 Extracellular diffusion of glutamate and receptor occupancy following synaptic activation. (*A1–3*) Glutamate concentrations shown in the central plane perpendicular to the synaptic cleft, at 1.0 ms post-release, for three characteristic cases of glial coverage (as indicated by dot-filled segments): no glia (*A1*), 50% of the synapse (postsynaptic structures only) is covered by glia (*A2*), 95% of the synapse is covered (*A3*); axis ticks, 0.1 μm. (*B1–3*) Time course of extracellular glutamate at five location, as shown by arrows in *A1*: 1, cleft center; 2, cleft edge; 3, inside the glial sheath adjacent to the postsynaptic hemisphere; 4, 0.5 μm presynaptically; 5, 0.5 μm postsynaptically. (*C1–3*) Occupancy time course for low- (*C*, K_d = 300 μM) and high- (*D*, K_d = 1 μM) affinity, singly bound receptors at five spatial locations, as shown in *A1*. Five thousand molecules of glutamate are released; density of available GLT/GLAST transporters on glia surfaces is $5 \cdot 10^3$ μm^{-2}; D = 0.3 μm^2/ms. See text for other parameters.

where square brackets indicate the extracellular concentration, indices show the time point, and $[T_{tot}]$ is the total concentration of transporters.

Occupancy of glutamate receptors

At each spatial compartment, the occupancy of glutamate receptor binding sites (singly bound) at various distances from the release site, $[Glu_{bo}]$, was computed from the simple reaction

$$Glu_{free} \underset{k^*_{-1}}{\overset{k^*_1}{\longleftrightarrow}} Glu_{bo} \quad (4a)$$

in the form of an explicit finite-difference scheme

$$[Glu_{bo}]_t = [Glu_{bo}]_{t-dt} + \{k^*_1[Glu_{free}]_{t-dt}([R_{tot}] - [Glu_{bo}]_{t-dt}) - k^*_{-1}[Glu_{bo}]_{t-dt}\}dt \quad (4b)$$

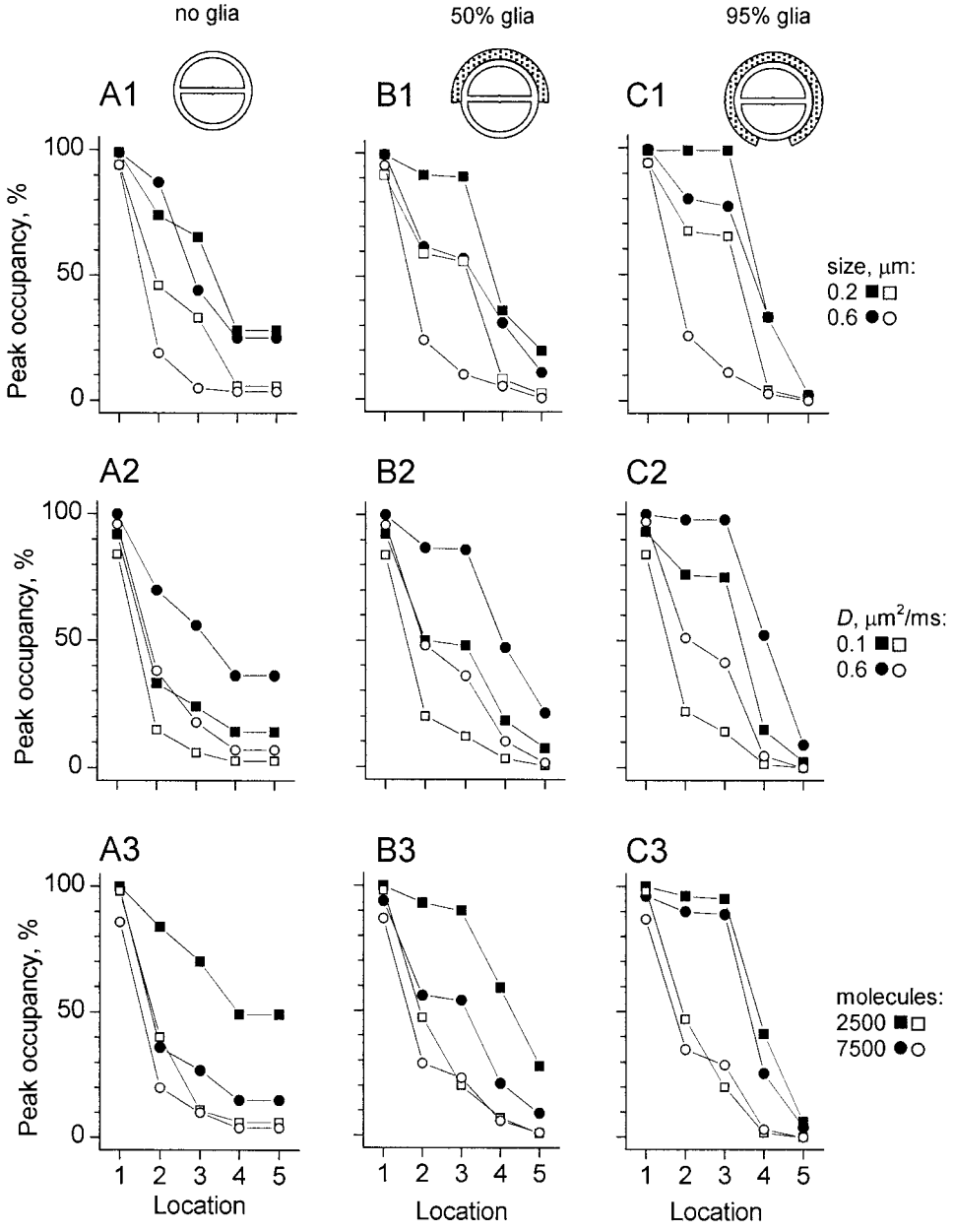

FIGURE 3 Peak occupancy of low- (*open symbols*) and high- (*solid symbols*) affinity receptors for different synaptic sizes (*A1–C1*) and at the likely physiological limits of glutamate diffusivity (*A2–C2*) and synaptic vesicle content (*A3–C3*). Five spatial locations (shown by arrows in Fig. 2, *A1*) are illustrated for the three characteristic cases of glial coverage, as illustrated in upper panels (or in Fig. 2) by dotted segments: no glia (*A1–3*), 50% (*B1–3*), and 95% of glial coverage (*C1–3*). (*A1–C1*) Synaptic diameter was set at 0.2 μm (*squares*) or 0.6 μm (*circles*). (*A2–C2*) Effective diffusion coefficient of glutamate was set at 0.1 μm^2/ms (*squares*) or 0.6 μm^2/ms (*circles*). (*C*) Synaptic vesicle content was set at 2500 (*squares*) or 7500 (*circles*) glutamate molecules.

where $[R_{tot}]$ = const is the total level of receptor binding sites (cancelled in relative measures), and $k^*_{1\ \text{and}}\ k^*_{-1}$ represent the receptor binding and unbinding rates, respectively. Equation 4b assumes that binding to glutamate receptors has a negligible effect on the glutamate level $[Glu_{free}]$. Indeed, the calibrated immunogold labeling of fast ionotropic glutamate receptors indicates that synapses in the hippocampus contain, on average, 10–15 AMPA receptors (Takumi et al., 1999; Nusser et al., 1998), and three to four times more NMDA receptors (Takumi et al., 1999; Racca et al., 2000). Because the average 3D diameter of synaptic clefts in this area is ~0.25 μm (Rusakov et al., 1998), the level of AMPA and NMDA receptors inside the cleft should be 20–30 and 60–90 μM, respectively. However, the synaptic clefts occupy only 1–2% of the extracellular space (Rusakov et al., 1998), and the occurrence of these receptors appears to be much lower outside the cleft (Takumi et al., 1999; Nusser et al., 1998; Racca et al., 2000). This implies that the average extracellular level of these receptors is unlikely to exceed 1–10 μM, which is negligible compared to the level of glutamate transporters (see above). Therefore, function $[Glu_{free}](t)$ in Eq. 4b was computed directly from the diffusion-uptake simulations described in previous sections.

Two characteristic types of glutamate receptor binding sites were considered: a low-affinity site (K_d = 300 μM, $k^*_1 = 10^4$ M^{-1} ms^{-1}, k^*_{-1} = 3 ms^{-1}) compatible with the properties of AMPA receptors (Jonas et al., 1993); and, separately, a high-affinity site (K_d = 1 μM, $k^*_1 = 7 \cdot 10^3$ M^{-1} ms^{-1}, k^*_{-1} = 0.007 ms^{-1}), compatible with NMDA receptors (Lester and Jahr, 1992). For the sake of clarity, the occupancy of singly bound sites was illustrated; the occupancy of *n*-bound receptors (assuming independent binding sites) can be calculated from these data by raising the values to the *n*th power.

Presynaptic calcium influx

A similar compartmental model of the synaptic environment was adopted to address depletion of extracellular Ca^{2+} near central synapses. The resting level of extra and intracellular Ca^{2+} was set at 1.3 mM and 0.1 μM, respectively. For the sake of simplicity, presynaptic Ca^{2+} channels were distributed evenly within the synaptic apposition zone, and their kinetics were set to follow the action potential (AP) time course:

$$Q(t) = mQ_0\phi t \exp(-\phi t), \quad (5)$$

where $Q_0 = I/(ZeN_A)$, I = 0.5 pA is the typical single Ca^{2+} channel peak current parameter; Z = 2 for Ca^{2+}; $e = 1.9 \cdot 10^{-19}$ C is the elementary charge; $N_A = 6 \cdot 10^{23}$ mol^{-1} is Avogadro's number; ϕ = 10 ms^{-1} (Helmchen et al., 1997; Sabatini and Regehr, 1998); and m is the total number of channels in the presynaptic membrane. In this model, the single-channel kinetics simply reflected the population behavior of Ca^{2+} channels (with a single channel transferring $\sim 5 \cdot 10^{-4}$ pC over the opening period). Therefore, the Ca^{2+} influx kinetics were dictated here by the known kinetics of the Ca^{2+} currents, which have been measured in electrophysiological experiments, rather than by the microscopic biophysical properties of individual channels.

The number of functional Ca^{2+} channels per synapse m is generally unknown, and, furthermore, may vary across the synaptic population (see Sabatini and Svoboda, 2000, for most recent estimates). It is clear, however, that m should critically determine the extent of Ca^{2+} depletion at each particular synapse. Conversely, the synaptic environment could be characterized by how many open channels would deplete Ca^{2+} in the cleft. The latter approach was adopted in the present study: for each characteristic synaptic environment a value of m_{50} was established, which corresponded to the 50% (peak) Ca^{2+} depletion at the synaptic cleft center (the value of 50% was chosen because complete depletion of the ion would not be compatible with a sustained Ca^{2+} current).

Postsynaptic calcium influx

The time course of postsynaptic Ca^{2+} influx (in subthreshold conditions) was set to follow the characteristic kinetics of the NMDA receptor current (Zador and Koch, 1994):

$$J(t) = J_0\{\exp(-t/\tau_1) - \exp(-t/\tau_2)\} \quad (6)$$

where J_0 is the current density parameter, τ_1 = 80 ms and τ_2 = 3 ms (for instance, J_0 = 1 pA/μm^2 corresponds to a charge transfer density of $\sim$0.07 pC/μm^2 over 200 ms). As in the case of presynaptic influx (see above), the critical unknown variable was J_0, and the characteristic value J_{50}, at which the peak depletion at the cleft center was 50%, was established for each type of the synaptic environment. Because electron immunogold labeling of NMDA receptors indicates that the occurrence of synaptic ionotropic receptors is much lower outside the cleft than inside (Nusser et al., 1998; Takumi et al., 1999; Racca et al., 2000), postsynaptic Ca^{2+} influx in the present simulations was also restricted to the membrane facing the cleft.

Ca^{2+} extrusion

The rate of active Ca^{2+} extrusion from the cytoplasm through metabolic pumps was approximated by the expression $S_V P_m C$, where S_V is the volume density of cell surfaces (estimated as 14 $\mu m^2/\mu m^3$ for neuropil in hippocampus (Rusakov and Kullmann, 1998a) and cerebellum (Lehre and Danbolt, 1998)), $P_m \sim 0.1$–0.2 μm/ms is the membrane pump parameter, and $C \sim 0.1$–1.0 μM is a factor that determines the pump kinetics (Zador and Koch, 1994). At physiological levels of intracellular Ca^{2+}, this rate estimate is compatible with the first-order Ca^{2+} extrusion rate of 0.4–0.9 ms^{-1} measured in real-time physiological observations of presynaptic terminals in the brain stem (Helmchen et al., 1997). The average rate of Ca^{2+} extrusion was in the range of 1 μM/ms; its effect on extracellular Ca^{2+} transients was considered negligible.

Ca^{2+} diffusion in a calyx-type synapse

The geometry of the model was modified to match the morphology of calyx-type synapses, as illustrated in Fig. 6 *A*. In agreement with experimental observations (Stanley, 2000; Borst and Sakmann, 1999), the external radius of the calyx was set at R_o = 10 μm, and the synaptic cleft had the same spatial curvature to form near-spheric calyceal shape (Fig. 6 *A*). The cleft width was initially set at 30 nm (Stanley, 2000), and the impact of cleft widening was tested by increasing this value up to 200 nm. The diffusion coefficient of Ca^{2+} in the cleft was set close to its free-medium value, 0.7 μm^2/ms. Where specified, a 0.2 μm wide glial sheath was "constructed" around the calyx (leaving a 100-nm extracellular gap and two 2-μm-wide openings at the "poles" of the calyx). The simulated kinetics of pre and postsynaptic Ca^{2+} channels were similar to those adopted at small central synapses (see Eqs. 5 and 6). In this study, glutamate diffusion within the calyx was not investigated, as this would require a more accurate knowledge about the distribution and properties of release sites and glutamate transporters within the synapse.

Ca^{2+} transients on the scale of multiple synapses

To assess the extent and kinetics of Ca^{2+} depletion in a relatively large area of neuropil during synchronous firing of multiple synapses, Ca^{2+} influx was set to occur homogeneously within a 10-μm-wide spherical area of a porous medium (α = 0.12; λ = 1.4, see above). The Ca^{2+} influx density was computed based on the reported stereological data, which show that 1 μm^3 of hippocampal neuropil contains, on average, 14 μm^2 of cell membranes (Rusakov and Kullmann, 1998a; Rusakov et al., 1998), half of which was assumed to carry Ca^{2+} channels. To mimic a short burst of synaptic activity originating at a distant neuronal pool, the Ca^{2+} influx kinetics followed function (6) with τ_1 = 10 ms and τ_2 = 3 ms, and the characteristic value of J_{50}, at which a 50% depletion of the ion is observed at the center of the area, was established in a series of simulation runs.

Mass conservation

In simulations of glutamate diffusion and uptake, the total of free, bound, and the time-integrated amount of transported glutamate across all (i, j)th compartments was computed at each time point t using the expression (see previous sections for notations):

$$\sum_{i,j}\left\{[\mathrm{Glu}](i,j,t) + [\mathrm{Glu}T](i,j,t) + \int_0^t k_2[\mathrm{Glu}T](i,j,t')dt'\right\}V(i,j) \quad (7)$$

and compared with the total number of released molecules (measuring unit factors are omitted).

Similarly, the space-integrated Ca^{2+} depletion was compared with the time-integrated amount of Ca^{2+} that has been lost from the extracellular space due to its pre or postsynaptic influx at each time step:

$$\sum_{i,j}\{[Ca^{2+}]_\infty - [Ca^{2+}]_0(i,j,t)\}V(i,j) = \sum_{i,j} V(i,j)\int_0^t \{J_{PRE}(i,j,t') + J_{POST}(i,j,t')\}dt' \quad (8)$$

where $[Ca^{2+}]_\infty$ is the resting level and J_{PRE} and J_{POST} are the rate of the pre- and postsynaptic Ca^{2+} influx, respectively.

The relationships (7) and (8) were monitored to confirm that the diffusion-reaction algorithm was accurate (without stepwise normalization of the conserved mass) for the required computing period and the appropriate cutoff distance.

RESULTS

Glutamate escape from glial envelope

The shades of gray in Fig. 2, *A1–3* illustrate the computed concentration of extracellular glutamate in the central plane perpendicular to the synaptic cleft (consistent with Fig. 1 *B*) at $t = 1$ ms for the three characteristic cases of glial coverage, as indicated. The corresponding time course of glutamate transient sampled at five spatial locations (shown in *A1* by arrows) is depicted in Fig. 2, *B1–3*, and Fig. 2, *C1–3* depicts the corresponding occupancy of singly bound low- and high-affinity receptors. The results predict that, despite high levels of glutamate transporters in glial membranes, the presence of glial sheaths does increase both the peak levels and the slow component of glutamate transient within and near the synaptic cleft. The occupancy of high-affinity receptors appears more sensitive to glial coverage than that of low-affinity receptors.

In these simulation experiments the synaptic size (diameter ~0.4 μm) represented the morphology of the parallel fiber synapse in cerebellum (Castejon and Castejon, 1997; Castejon, 1990; Lehre and Rusakov, unpublished observations). We asked whether the size affects the relationship between glutamate spillover and glia. Fig. 3, *A1–C1* shows the peak occupancy levels of low- and high-affinity receptors for the synaptic diameter of 0.2 μm, which is compatible with excitatory synapses in hippocampal area CA1 (Shepherd and Harris, 1998; Rusakov et al., 1997), or 0.6 μm, which is compatible with the climbing fiber synapses in cerebellum (Castejon and Castejon, 1997; Castejon et al., 1994). Fig. 3, *A2–C2* addresses the uncertainty about the diffusion coefficient of glutamate: the peak occupancy levels were computed for the likely lower and upper physiological limits of D, 0.1 μm^2/ms and 0.6 μm^2/ms, respectively. There is no universal agreement about the synaptic vesicle content, and data in Fig. 3, *A3–C3* illustrate the peak receptor occupancy at two different values of the vesicle content, 2500 and 7500 molecules. These results demonstrate that a wide range of receptor occupancies can be found in the synaptic vicinity and that the effects of glial coverage remain qualitatively similar over the physiological range of D and vesicle content.

Ca^{2+} depletion and glial sheaths

Fig. 4, *upper panels*, depicts the computed time course of $[Ca^{2+}]_o$ at five perisynaptic locations (arrows in Fig. 2 *A1*) following the AP-driven activation of presynaptic channels for the three characteristic cases of glial coverage (*A–C*), with the Ca^{2+} influx parameter m (Eq. 5) set at its characteristic value of m_{50} (which corresponds to a 50% peak depletion at the cleft center, see Methods), as shown. Correspondingly, Fig. 4, *A–C*, *lower panels*, shows the time course of Ca^{2+} depletion induced by the NMDAR kinetics-driven postsynaptic channels at the characteristic current density J_{50}. The data predict that increasing glial coverage reduces dramatically the magnitude of postsynaptic Ca^{2+} influx required to deplete Ca^{2+} in the cleft (compare J_{50} in lower panels), whereas the effect is small when the Ca^{2+} influx kinetics are fast (compare m_{50} in upper panels).

As in the previous sections, the relationship between glia and Ca^{2+} depletion was investigated for two other synaptic diameters (0.2 μm and 0.6 μm), and the corresponding values of m_{50} and J_{50} are shown in Fig. 5, *A* and *B*. To address some uncertainty regarding diffusion coefficient D, Fig. 5, *C* and *D* depicts the computed values of m_{50} and J_{50} at the likely extremes of the extracellular Ca^{2+} diffusion coefficient, 0.1 μm^2/ms and 0.7 μm^2/ms (Nicholson et al., 1978; Nicholson and Rice, 1987). The results indicate that larger synapses are more likely to exhibit Ca^{2+} depletion caused by the slow postsynaptic, but not fast presynaptic, sinks (compare *A* and *B*), and that slowing down diffusion sevenfold corresponds to a four to fivefold facilitation of depletion (*C* and *D*).

Ca^{2+} depletion in a calyx-type synapse

The compartmental model of the calyx synapse is schematically depicted in Fig. 6 *A* (see Methods for details). Fig. 6 *B* shows the time course of Ca^{2+} depletion caused by the AP-driven channels at five different synaptic locations, indicating that m_{50} and J_{50} for this synapse (without glial coverage) are 47,500 and 0.103 pA/μm^2, respectively. Characteristically, the time course of Ca^{2+} depletion was an order of magnitude slower than the underlying presynaptic Ca^{2+} influx (*dotted line* in Fig. 6*B*, *lower panel*). The effect of the glial sheaths is addressed in Fig. 6 *C*, predicting that they should mainly increase the slow decay component of depletion. There is some uncertainty about the cleft width in

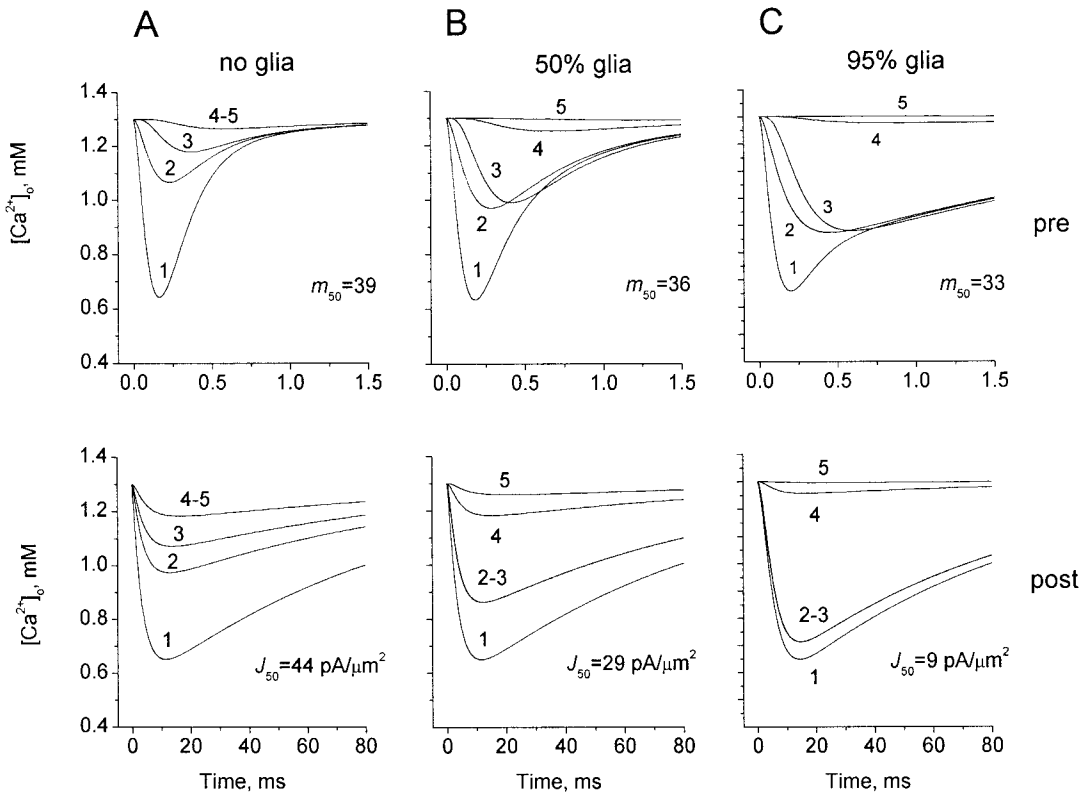

FIGURE 4 The relationship between glial coverage and Ca^{2+} depletion induced by synaptically activated Ca^{2+} influx. Plots illustrate the time course of $[Ca^{2+}]_o$ at five perisynaptic locations (arrows in Fig. 2, *A1*) for three cases of glial coverage (shown in Fig. 3 by dotted segments): no glia (*A*), 50% (*B*), and 95% of glial coverage (*C*) following the opening of presynaptic, AP-driven (*upper panels*) or postsynaptic, NMDAR-driven (*lower panels*) channels. In each case the characteristic parameters of Ca^{2+} influx, m_{50} or J_{50}, are shown, which correspond to a 50% depletion at the cleft center, as explained in Methods. Synaptic diameter was set at 0.2 μm, $D = 0.4$ μm^2/ms.

this type of synapses, and data in Fig. 6 *D* show simulation results for the average width increased up to 60 nm: the resulting Ca^{2+} transient indicates a reduced (to 26%) depletion in the cleft center. Further increases in the cleft width correspond to a steep attenuation of any Ca^{2+} depletion: given the unchanged Ca^{2+} influx, a 200-nm-wide cleft

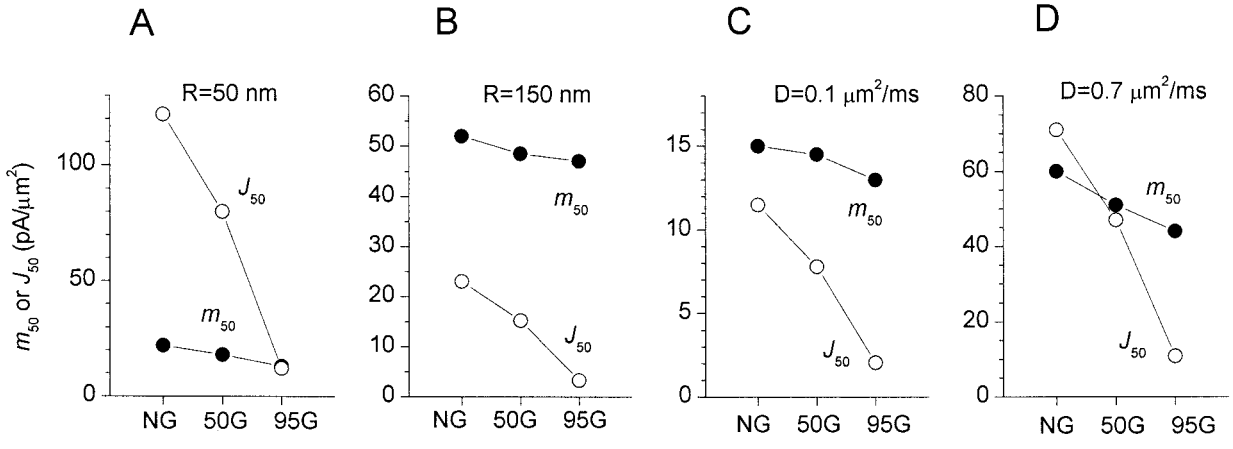

FIGURE 5 The effect of synaptic size and extracellular diffusivity on synaptically evoked Ca^{2+} depletion. Plots show the characteristic number of presynaptic channels m_{50} (*filled circles*) and postsynaptic peak current density parameter J_{50} (*open circles*) that correspond to a 50% depletion at the cleft center for synaptic diameters of 0.1 μm (*A*) and 0.3 μm (*B*) and diffusion coefficients of 0.1 μm^2/ms (*C*) and 0.7 μm^2/ms (*D*). Three cases of glial coverage are shown (illustrated in Fig. 3, dotted segments), as denoted in the abscissa: NG, no glia; 50G, 50% glial coverage; 95G, 95% glial coverage.

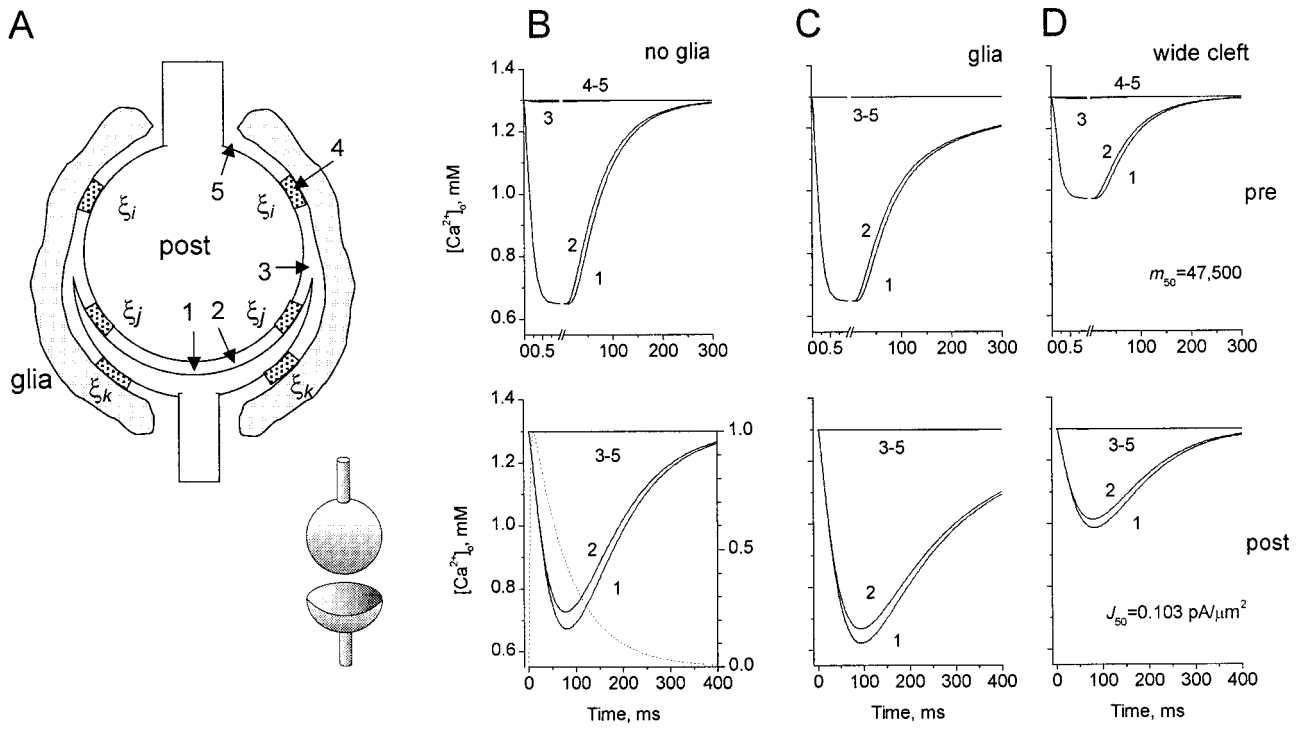

FIGURE 6 Synaptically evoked transients of Ca^{2+} at the calyx-type synapse. (*A*) Diagram illustrating a central planar section of a 3D compartmental model of the calyx synapse; ξ_i–ξ_k exemplify sections of three individual space compartments. (*B*) Time course of Ca^{2+} depletion in response to fast presynaptic (*upper panel*, not two-scale abscissa) or NMDAR-driven postsynaptic (*lower panel*) Ca^{2+} influx at five spatial locations as indicated by arrows in *A*: 1, cleft center; 2, 3 μm laterally in the cleft; 3, at the cleft edge; 4, half-way through the calyx sphere; 5, at the calyx "pole." Synaptic cleft width is 30 nm. No glia is present. Dotted line (*lower panel*) shows the time course of Ca^{2+} influx. (*C*) Conditions and notations are as in *B* except that a 0.2-μm-wide glial sheath surrounds the calyx. (*D*) Conditions and notations are as in *B* except for a 60-nm-wide synaptic cleft. The characteristic current density parameter (m_{50} and J_{50} for pre and postsynaptic influx, respectively, shown in (*D*) corresponds to a 50% depletion of the ion in the cleft center in case *B*, and was not changed in *C* and *D*.

would allow only a 4% Ca^{2+} depletion in the cleft center (data not shown).

Ca^{2+} depletion following activation of multiple synapses

The results described above have addressed Ca^{2+} depletion near individual synapses. We then asked whether a significant depletion can be expected when multiple synapses are activated in the neuropil. As detailed in Methods, this was achieved by simulating Ca^{2+} influx over a 10-μm-wide (spherical) area of a porous medium (kinetics shown by dotted line in Fig. 7 *A*). The resulting time course of $[Ca^{2+}]_o$ and its spatial profile at $t = 20$ ms (time point close to the peak depletion) are depicted in Fig. 7, *A* and *B*, respectively. As in the case of the calyx-type synapse, the data predict a strong temporal filtering of the $[Ca^{2+}]_o$ transient (compare *dotted* and *solid lines* in Fig. 7 *A*) and a relatively small extent of depletion beyond the boundary of open Ca^{2+} sinks (Fig. 7 *B*).

DISCUSSION

Glutamate diffusion inside and outside glial sheath

The present results indicate that glial sheaths have a profound effect on the activation profile of perisynaptic receptors. Covering one-half of the synaptic structures with glia increases the glutamate concentration inside the sheath almost twofold, while outside the sheath the concentration drops two to fourfold (Fig. 2, *A2–B2*). If glia cover ~95% of the synapse, glutamate inside the envelope remains at a high level (20–50 μM) for >10 ms post-release; this corresponds to a 10- to 100-fold concentration difference between the inner and outer sides of the glial sheath (Fig. 2, *A3–B3*).

In line with the earlier findings (Rusakov and Kullmann, 1998a), simulation results in Fig. 2, *C1–3* indicate that the occupancy of low-affinity receptors falls much steeper with greater distances from the release site than does the occupancy of high-affinity receptors. Increasing the glial coverage results in a 50–100% increase in the occupancy of high-affinity sites inside the shield (ap-

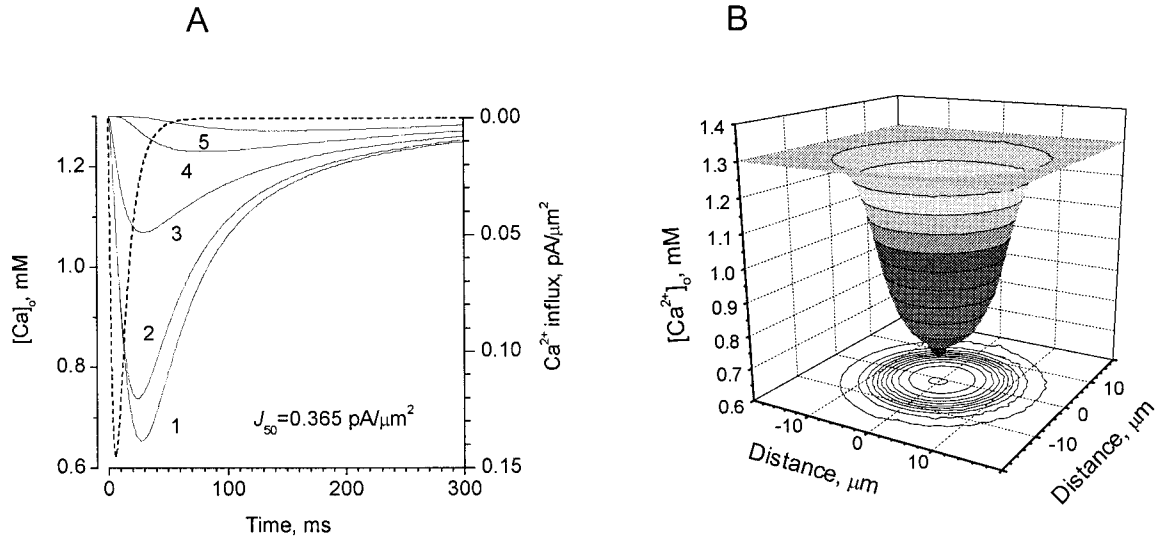

FIGURE 7 Ca^{2+} transient in synaptic neuropil in response to a brief wave of Ca^{2+} influx across a 10-μm-wide volume. (*A*) Time course of Ca^{2+} depletion (characteristic influx parameter J_{50} is shown) at five distances d from the center: 0, 5, 10, 15, and 20 μm, respectively. Dashed line shows the time course of Ca^{2+} influx current (Eq. 6; $\tau_1 = 10$ ms, $\tau_2 = 3$ ms). (*B*) The spatial profile of Ca^{2+} depletion at $t = 20$ ms after the Ca^{2+} influx onset.

proaching the saturation level), whereas the low-affinity sites appear to be much less affected (Fig. 2, *C1–3*). Qualitatively similar phenomena can be predicted for different synaptic sizes and at the likely physiological limits of the glutamate diffusivity and synaptic vesicle content (Fig. 3). Interestingly, the high-affinity sites located outside the glial shield opening (at 0.5 μm from the release site) show significant occupancy levels (up to 20–30%) even at the ~95% glial coverage (see location 4 in Fig. 2 *C3* and Fig. 3 *C1–3*). Given that a distance of 0.5 μm is compatible with the nearest neighbor distance between hippocampal synapses (Rusakov et al., 1998; Rusakov and Kullmann, 1998a), this suggests that even the tight glial sheath enriched in transporters does not entirely prevent activation of high-affinity (in contrast to low-affinity) receptors at the neighboring synapses via glutamate escape.

It has recently been shown that, at the stratum radiatum synapse in the hippocampus, the NMDA receptor-dependent Ca^{2+} influx into dendritic spines does not appear to occlude at short intervals (~15 ms) between stimulation pulses (Mainen et al., 1999), implying that these receptors are not saturated. Interestingly, the present simulation data predict that the occupancy of both low- and high-affinity sites may vary significantly, even in the immediate synaptic vicinity, depending on the distance from the release site and on the glial coverage (Figs. 2 and 3). This suggests that the occupancy of NMDA receptors estimated in electrophysiological experiments may represent the average value over a wide range of occupancies, both inside and outside the synaptic cleft.

Calcium depletion

The synaptic cleft volume at common excitatory synapses ranges between $\sim 5 \cdot 10^{-4}$ μm^3 (hippocampal area CA1) and $5 \cdot 10^{-3}$ μm^3 (climbing fiber synapses in cerebellum), which was represented by the assumptions of the present model. This implies that the synaptic cleft accommodates, on average, 10^{-4}-10^{-3} pC of free Ca^{2+} ions (at 1 mM). The density of voltage-gated Ca^{2+} channels in dendritic spines of hippocampal neurons has recently been estimated (using a two-photon excitation Ca^{2+} imaging) to be in the range of 20 μm^{-2}, each spine containing one to 20 channels (Sabatini and Svoboda, 2000). Similar Ca^{2+} channel densities (the range of 1–55 μm^{-2}) were reported to occur in the presynaptic membrane of the calyx synapse in the chick ciliary ganglion (Haydon et al., 1994). Given the characteristic current through individual channel of 0.2–0.5 pA, these data correspond to the Ca^{2+} influx current density of 10–30 pA/μm^2. The present simulation results therefore predict that, in addition to a very brief (<1 ms scale) transient, significant Ca^{2+} depletion could indeed occur in small central synapses, which are only partly covered by glia, at the physiological level of Ca^{2+} influx and over the range of plausible synaptic architectures (Fig. 4, *B* and *C*; Fig. 5). These estimates are also consistent with the prediction that the back propagating action potentials in dendrites (driven by voltage gated Ca^{2+} channels) could partly deplete extracellular Ca^{2+} (Egelman and Montague, 1998).

Our results suggest that the extent of brief Ca^{2+} depletion induced by the AP-driven channels is much less affected by glial coverage at larger, as opposed to smaller, synapses (compare Fig. 5, *A* and *B*, *filled circles*). The impact of glia,

however, becomes prominent when the kinetics of Ca^{2+} sinks is slow, as in the case of the postsynaptic NMDAR-dependent Ca^{2+} current (Fig. 5, *A* and *B*, *open circles*).

Calyceal synapse

The giant calyx-type synapse is a useful experimental model where channel currents and ion fluxes could be investigated in the conditions of pre and/or postsynaptic voltage clamp. In the brain stem MNTB synapse, Ca^{2+} depletion in the cleft was suggested to underlie the attenuated Ca^{2+} influx, which was observed when the synaptic membrane was depolarized for ~100 ms (Borst and Sakmann, 1999). This depolarization, which results in an accumulated Ca^{2+} influx of ~100 pC (Borst and Sakmann, 1999), corresponds either to an integrated influx over $n = 2 \cdot 10^5$ brief openings of AP-driven channels or to the postsynaptic current density parameter $J_0 = 1.5$ pA/μm^2 (over a membrane area of ~1000 μm^2) in the present model. The experimentally estimated magnitude of the Ca^{2+} influx appears, therefore, at least an order of magnitude higher than the influx that, according to the present simulations, should induce significant depletion of the ion (Fig. 6, *B* and *C*). One explanation of this discrepancy is that the synaptic cleft contains a significant amount of bound extracellular Ca^{2+} which, as suggested earlier (Borst and Sakmann, 1999), may become rapidly unbound following a drop in $[Ca^{2+}]_o$. Another possible explanation is simply that portions of the calyceal synaptic cleft are much wider than 30–50 nm and/or that real Calyx of Held terminals have a claw-like (or tulip-like), rather than cup-like, shape, which would enlarge the entrance routes for Ca^{2+} (or escape routes for glutamate). For instance, the present model predicts that increasing the synaptic cleft width could substantially reduce the extent of depletion (compare Fig. 6, *C* and *D;* also see Results), or, in other terms, increase the Ca^{2+} influx required for significant depletion to occur.

In fact, in the chick ciliary ganglion calyx synapse, a much smaller influx (<~2 pC) was reported to induce a significant depletion of Ba^{2+} (substitute for Ca^{2+} ions), as estimated by the difference in the post-depolarization tail current between terminals that did and did not have the attached postsynaptic cell (Stanley, 2000). These data suggest that Ca^{2+} depletion could be caused by an average Ca^{2+} influx in the range of 0.02 pA/μm^2 (over 100 ms assuming the influx area of 1000 μm^2). The simplest explanation for the apparent inconsistency between the two experimental observations is that the synaptic cleft is narrower (or better preserved) in the ciliary ganglion synapse. If so, this could also explain why the present model may underestimate Ca^{2+} depletion in this synapse (data in Fig. 6 here predict $J_{50} = 0.103$ pA/μm^2, which corresponds to an average current density of ~0.06 pA/μm^2 over a 100-ms period). It has been reported that the lateral pattern of Ca^{2+} channels in the presynaptic membrane of the ciliary ganglion calyx is highly inhomogeneous (Haydon et al., 1994). The latter implies that the areas with a high channel density may create local "depletion pools" within the cleft (similar to the effect at small synapses, see Figs. 2 and 3; see also Discussion in Stanley, 2000). If so, the reduction in the tail Ca^{2+} current (that flows through the same local channels) will be exaggerated. Any substantial increases in the synaptic cleft width would, however, diminish these local nonhomogeneities, and thus approach the case of the uniform distribution of Ca^{2+} channels, which is more accurately presented by the present model.

Multiple synapses

Data in Fig. 7 predict that the Ca^{2+} influx at a density of 0.3–0.4 pA/μm^2 in synaptic neuropil could be sufficient to induce a significant depletion on a macroscopic (~10 μm) scale. Is this Ca^{2+} influx physiologically plausible? The model parameters here adopt the stereological quantities of the hippocampal neuropil, in which 1 μm^3 contains, on average, ~14 μm^2 of cell membranes (half of which is assumed postsynaptic), and ~2 synaptic contacts (Rusakov and Kullmann, 1998a; Rusakov et al., 1998). This implies that, for significant depletion to occur, Ca^{2+} influx should be 2–3 pA, or in the range of 10–20 Ca^{2+} channels, per 1 μm^3 of neuropil. Because it is unlikely that there are more than 10–20 voltage-dependent Ca^{2+} channels (Sabatini and Svoboda, 2000) and 30–40 NMDA receptors (Takumi et al., 1999; Racca et al., 2000) in the vicinity of individual hippocampal synapses, significant Ca^{2+} depletion would require a substantial proportion (10–20%) of local synapses to be activated simultaneously. This appears to be in general agreement with predictions of a compartmental model reported earlier (Egelman and Montague, 1998, 1999). Although such a strong activation would be difficult to achieve in a brain slice experiment, it remains to be elucidated whether this situation can occur in vivo.

CONCLUDING REMARKS

The present study uses a novel compartmental model to address a simple question: How strongly do transients of glutamate and Ca^{2+} depend on glial coverage? What properties of the synaptic environment determine this dependence? The results give a quantitative account of how glial sheaths of central synapses can shape the perisynaptic transient of glutamate and facilitate depletion of Ca^{2+} in the synaptic cleft at physiological levels of glutamate uptake and Ca^{2+} influx. Detailed modeling of the calyx-type synapse geometry predicted a significant temporal filtering of Ca^{2+} depletion in this synapse; this phenomenon is also illustrated for fast Ca^{2+} influx in the neuropil on a larger (>10 μm) scale. The obtained results therefore provide quantitative guidance for interpretation of physiological ex-

periments that address fast extracellular transients of neurotransmitters and small ions in the brain tissue.

The author is grateful to Drs. D. M. Kullmann, K. P. Lehre, and A. Fine for their valuable comments regarding this study.

This work was supported by the MRC Career Development Award G120/490 (UK).

REFERENCES

Araque, A., V. Parpura, R. P. Sanzgiri, and P. G. Haydon. 1999. Tripartite synapses: glia, the unacknowledged partner. *Trends Neurosci.* 22: 208–215.

Arriza, J. L., W. A. Fairman, J. I. Wadiche, G. H. Murdoch, M. P. Kavanaugh, and S. G. Amara. 1994. Functional comparison of three glutamate transporter subtypes cloned from human motor cortex. *J. Neurosci.* 14:5559–5569.

Asztely, F., G. Erdemli, and D. M. Kullmann. 1997. Extrasynaptic glutamate spillover in the hippocampus: dependence on temperature and the role of active glutamate uptake. *Neuron.* 18:281–293.

Auger, C., and D. Attwell. 2000. Fast removal of synaptic glutamate by postsynaptic transporters. *Neuron.* 28:547–558.

Barbour, B., B. U. Keller, I. Llano, and A. Marty. 1994. Prolonged presence of glutamate during excitatory synaptic transmission to cerebellar Purkinje cells. *Neuron.* 12:1331–1343.

Bartol, T. M., B. R. Land, E. E. Salpeter, and M. M. Salpeter. 1991. Monte Carlo simulation of miniature endplate current generation in the vertebrate neuromuscular junction. *Biophys. J.* 59:1290–1307.

Bergles, D. E., and C. E. Jahr. 1998. Glial contribution to glutamate uptake at Schaffer collateral-commissural synapses in the hippocampus. *J. Neurosci.* 18:7709–7716.

Borst, J. G. G., and B. Sakmann. 1999. Depletion of calcium in the synaptic cleft of a calyx-type synapse in the rat brain stem. *J. Physiol.* 521: 123–133.

Brown, E. M., P. M. Vassiliev, and S. C. Hebert. 1995. Calcium ions as extracellular messengers. *Cell.* 83:679–682.

Bruns, D., and R. Jahn. 1995. Real-time measurement of transmitter release from single synaptic vesicles. *Nature.* 377:62–65.

Carter, A. G., and W. G. Regehr. 2000. Prolonged synaptic currents and glutamate spillover at the parallel fiber to stellate cell synapse. *J. Neurosci.* 20:4423–4434.

Castejon, O. J. 1990. freeze-fracture scanning electron-microscopy and comparative freeze-etching study of parallel fiber-Purkinje spine synapses of vertebrate cerebellar cortex. *J. Submicrosc. Cytol. Pathol.* 22:281–295.

Castejon, O. J., R. P. Apkarian, and C. Valero. 1994. Conventional and high-resolution scanning electron-microscopy and cryofracture techniques as tools for tracing cerebellar short intracortical circuits. *Scanning Microsc.* 8:315–324.

Castejon, O. J., and H. V. Castejon. 1997. Conventional and high resolution scanning electron microscopy of cerebellar Purkinje cells. *Biocell.* 21:149–160.

Clements, J. D. 1996. Transmitter timecourse in the synaptic cleft: its role in central synaptic function. *Trends Neurosci.* 5:163–170.

Diamond, J. S., and C. E. Jahr. 1997. Transporters buffer synaptically released glutamate on a submillisecond time scale. *J. Neurosci.* 17: 4672–4687.

Egelman, D. M., and P. R. Montague. 1998. Computational properties of peri-dendritic calcium fluctuations. *J. Neurosci.* 18:8580–8589.

Egelman, D. M., and P. R. Montague. 1999. Calcium dynamics in the extracellular space of mammalian neural tissue. *Biophys. J.* 76: 1856–1867.

Haydon, P. G., E. Henderson, and E. F. Stanley. 1994. Localization of individual calcium channels at the release face of a presynaptic nerve-terminal. *Neuron.* 13:1275–1280.

Helmchen, F., J. G. G. Borst, and B. Sakmann. 1997. Calcium dynamics associated with a single action potential in a CNS presynaptic terminal. *Biophys. J.* 72:1458–1471.

Isaacson, J. S. 1999. Glutamate spillover mediates excitatory transmission in the rat olfactory bulb. *Neuron.* 23:377–384.

Janigro, D., S. Gasparini, R. Dambrosio, G. McKhann, and D. Di Francesco. 1997. Reduction of K^+ uptake in glia prevents long-term depression maintenance and causes epileptiform activity. *J. Neurosci.* 17:2813–2824.

Jonas, P., G. Major, and B. Sakmann. 1993. Quantal components of unitary EPSCs at the mossy finre synapse on CA3 pyramidal cells of rat hippocampus. *J. Physiol.* 472:615–663.

King, R. D., M. C. West, P. R. Montague, and D. M. Egelman. 2000. Do extracellular Ca^{2+} signals carry information through the tissue? *Trends Neurosci.* 23:12–13.

Kleinle, J., K. Vogt, L. Müller, W. Senn, K. Wyler, and J. Streit. 1996. Transmitter concentration profiles in the synaptic cleft: an analytical model of release and diffusion. *Biophys. J.* 71:2413–2426.

Kruk, P. J., H. Korn, and D. S. Faber. 1997. The effects of geometrical parameters on synaptic transmission: a Monte Carlo simulation study. *Biophys. J.* 73:2874–2890.

Kuffler, S. W., J. G. Nicholls, and R. K. Orkand. 1966. Physiological properties of glial cells in the central nervous system of amphibia. *J. Neurophysiol.* 29:768–787.

Lehre, K. P., and N. C. Danbolt. 1998. The number of glutamate transporter subtype molecules at glutamatergic synapses: chemical and stereological quantification in young adult rat brain. *J. Neurosci.* 18: 8751–8757.

Lehre, K. P., L. M. Levy, O. P. Ottersen, J. Storm-Mathisen, and N. C. Danbolt. 1995. Differential expression of two glial glutamate transporters in the rat brain: quantitative and immunocytochemical observations. *J. Neurosci.* 15:1835–1853.

Lester, R. A. J., and C. E. Jahr. 1992. NMDA channel behavior depends on agonist affinity. *J. Neurosci.* 12:635–643.

Mainen, Z. F., R. Malinow, and K. Svoboda. 1999. Synaptic calcium transients in single spines indicate that NMDA receptors are not saturated. *Nature.* 399:151–155.

Mennerick, S., W. X. Shen, W. Y. Xu, A. Benz, K. Tanaka, K. Shimamoto, K. E. Isenberg, J. E. Krause, and C. F. Zorumski. 1999. Substrate turnover by transporters curtails synaptic glutamate transients. *J. Neurosci.* 19:9242–9251.

Mitchell, S. J., and R. A. Silver. 2000a. GABA spillover from single inhibitory axons suppresses low- frequency excitatory transmission at the cerebellar glomerulus. *J. Neurosci.* 20:8651–8658.

Mitchell, S. J., and R. A. Silver. 2000b. Glutamate spillover suppresses inhibition by activating presynaptic mGluRs. *Nature.* 404:498–502.

Mody, I., and U. Heinemann. 1986. Laminar profiles of the changes in extracellular calcium concentration induced by repetitive stimulation and excitatory amino acids in the rat dentate gyrus. *Neurosci. Lett.* 69:137–142.

Montague, P. R. 1996. The resource consumption principle: attention and memory in volumes of neural tissue. *Proc. Natl. Acad. Sci. U.S.A.* 93:3619–3623.

Nicholson, C. 1980. Modulation of extracellular calcium and its functional implications. *Fed. Proc.* 39:1519–1523.

Nicholson, C. 1995. Interaction between diffusion and Michaelis-Menten uptake of dopamine after iontophoresis in striatum. *Biophys. J.* 68: 1699–1715.

Nicholson, C., and M. E. Rice. 1987. Calcium diffusion in the brain cell microenvironment. *Can. J. Physiol. Pharmacol.* 65:1086–1091.

Nicholson, C., G. tenBruggencate, H. Stockle, and R. Steinberg. 1978. Calcium and potassium changes in extracellular microenvironments of cat cerebellar cortex. *J. Neurophysiol.* 41:1026–1039.

Nusser, Z., R. Lujan, G. Laube, J. D. B. Roberts, E. Molnar, and P. Somogyi. 1998. Cell type and pathway dependence of synaptic AMPA receptor number and variability in the hippocampus. *Neuron.* 21: 545–559.

Otis, T. S., and C. E. Jahr. 1998. Anion currents and predicted glutamate flux through a neuronal glutamate transporter. *J. Neurosci.* 18: 7099–7110.

Otis, T. S., and M. P. Kavanaugh. 2000. Isolation of current components and partial reaction cycles in the glial glutamate transporter EAAT2. *J. Neurosci.* 20:2749–2757.

Pumain, R., and U. Heinemann. 1985. Stimulus induced and amino acid induced calcium and potassium changes in rat neocortex. *J. Neurophysiol.* 53:1–16.

Racca, C., F. A. Stephenson, P. Streit, J. D. B. Roberts, and P. Somogyi. 2000. NMDA receptor content of synapses in stratum radiatum of the hippocampal CA1 area. *J. Neurosci.* 20:2512–2522.

Reichenbach, A. 1991. Glial K^+ permeability and CNS K^+ clearance by diffusion and spatial buffering. *Ann. N.Y. Acad. Sci.* 633:272–284.

Rossi, D. J., and M. Hamann. 1998. Spillover-mediated transmission at inhibitory synapses promoted by high affinity alpha(6) subunit GABA(A) receptors and glomerular geometry. *Neuron.* 20:783–795.

Rusakov, D. A., H. A. Davies, E. Harrison, G. Diana, G. Richter-Levin, T. V. P. Bliss, and M. G. Stewart. 1997. Ultrastructural synaptic correlates of spatial learning in rat hippocampus. *Neuroscience.* 80:69–77.

Rusakov, D. A., E. Harrison, and M. G. Stewart. 1998. Synapses in hippocampus occupy only 1–2% of cell membranes and are spaced less than half-micron apart: a quantitative ultrastructural analysis with discussion of physiological implications. *Neuropharmacology.* 37: 513–521.

Rusakov, D. A., and D. M. Kullmann. 1998a. Extrasynaptic glutamate diffusion in the hippocampus: ultrastructural constraints, uptake, and receptor activation. *J. Neurosci.* 18:3158–3170.

Rusakov, D. A., and D. M. Kullmann. 1998b. Geometric and viscous components of the tortuosity of the extracellular space in the brain. *Proc. Natl. Acad. Sci. U.S.A.* 95:8975–8980.

Rusakov, D. A., D. M. Kullmann, and M. G. Stewart. 1999. Hippocampal synapses: do they talk to their neighbours? *Trends Neurosci.* 22: 382–388.

Sabatini, B. L., and W. G. Regehr. 1998. Optical measurement of presynaptic calcium currents. *Biophys. J.* 74:1549–1563.

Sabatini, B. L., and K. Svoboda. 2000. Analysis of calcium channels in single spines using optical fluctuation analysis. *Nature.* 408:589–593.

Schousboe, A. 2000. Pharmacological and functional characterization of astrocytic GABA transport: a short review. *Neurochem. Res.* 25: 1241–1244.

Shepherd, G. M. G., and K. M. Harris. 1998. Three-dimensional structure and composition of CA3->CA1 axons in rat hippocampal slices: implications for presynaptic connectivity and compartmentalization. *J. Neurosci.* 18:8300–8310.

Smith, S. J. 1992. Do astrocytes process neural information? *Prog. Brain Res.* 94:119–136.

Spacek, J. 1985. Three-dimensional analysis of dendritic spines. 3. Glial sheath. *Anat. Embryol.* 171:245–252.

Stanley, E. F. 2000. Presynaptic calcium channels and the depletion of synaptic cleft calcium ions. *J. Neurophysiol.* 83:477–482.

Stiles, J. R., D. Van Helden, T. M. Bartol, E. E. Salpeter, and M. M. Salpeter. 1996. Miniature endplate current rise times <100 ms from improved dual recordings can be modeled with passive acetylcholine diffusion from a synaptic vesicle. *Proc. Natl. Acad. Sci. U.S.A.* 93: 5747–5752.

Sykova, E., T. Roitbak, T. Mazel, Z. Simonova, and A. R. Harvey. 1999. Astrocytes, oligodendroglia, extracellular space volume and geometry in rat fetal brain grafts. *Neuroscience.* 91:783–798.

Takumi, Y., V. Ramirez-Leon, P. Laake, E. Rinvik, and O. P. Ottersen. 1999. Different modes of expression of AMPA and NMDA receptors in hippocampal synapses. *Nature Neurosci.* 2:618–624.

Trommershauser, J., J. Marienhagen, and A. Zippelius. 1999. Stochastic model of central synapses: slow diffusion of transmitter interacting with spatially distributed receptors and transporters. *J. Theor. Biol.* 198: 101–120.

Uteshev, V. V., and P. S. Pennefather. 1996. A mathematical description of miniature postsynaptic current generation at central nervous system synapses. *Biophys. J.* 71:1256–1266.

Vassilev, P. M., J. Mitchel, M. Vassilev, M. Kanazirska, and E. M. Brown. 1997. Assessment of frequency-dependent alterations in the level of extracellular Ca^{2+} in the synaptic cleft. *Biophys. J.* 72:2103–2116.

Ventura, R., and K. M. Harris. 1999. Three-dimensional relationships between hippocampal synapses and astrocytes. *J. Neurosci.* 19: 6897–6906.

Wadiche, J. I., J. L. Arriza, S. G. Amara, and M. P. Kavanaugh. 1995. Kinetics of a human glutamate transporter. *Neuron.* 14:1019–1027.

Wahl, L. M., C. Pouzat, and K. J. Stratford. 1996. Monte Carlo simulation of fast excitatory synaptic transmission at a hippocampal synapse. *J. Neurophysiol.* 75:597–608.

Zador, A., and C. Koch. 1994. Linearized models of calcium dynamics: formal equivalence to the cable equation. *J. Neurosci.* 14:4705–4715.